JOURNAL OF MATERIALS SCIENCE **36** (2001) 2565–2570

Spectroscopic investigations of CdS nanoparticles in sol-gel derived polymeric thin films and bulk silica matrices

B. CAPOEN
Laboratoire de Physique des Lasers, Atomes et Molécules (CNRS, UMR 8523), Bât. P5 Centre d'Etudes et de Recherches Lasers et Applications (CERLA), Université de Lille 1, 59655 Villeneuve d'Ascq Cedex, France
E-mail: bruno.capoen@univ-lille1.fr

T. GACOIN
Laboratoire de Physique de la Matière Condensée (CNRS, UMR 7643), Ecole Polytechnique, 91128 Palaiseau Cedex, France

J. M. NÉDÉLEC
Laboratoire des Matériaux Inorganiques, Université Blaise Pascal, 24 avenue des Landais, 63177 Aubière, Cedex, France

S. TURRELL
Laboratoire de Spectrochimie Infrarouge et Raman (CNRS, UPRA 631L), Bât. C5 Centre d'Etudes et de Recherches Lasers et Applications (CERLA), Université de Lille 1, 59655 Villeneuve d'Ascq Cedex, France

M. BOUAZAOUI
Laboratoire de Physique des Lasers, Atomes et Molécules (CNRS, UMR 8523), Bât. P5 Centre d'Etudes et de Recherches Lasers et Applications (CERLA), Université de Lille 1, 59655 Villeneuve d'Ascq Cedex, France

Absorption, photoluminescence and Raman scattering spectroscopies have been performed on two kinds of SiO_2 bulk matrices and sol-gel polymeric thin films, containing CdS nanoparticles. Waveguiding in the polymeric CdS films has been demonstrated for wavelengths in the visible region. A simple surface energy diagram, including defect levels, has been used to explain the size-selective luminescence of the nanocrystals. The luminescence spectrum is composed of an excitonic recombination band and a broader red-shifted band, imputed to the transition between the surface trap levels. The particle interaction with the silica xerogels appears to enhance these surface states. Resonance Raman scattering shows that the excitons are coupled to LO-phonon modes, but the spectra exhibit no matrix effect on the frequency vibration of the fundamental LO phonon.

1. Introduction

Semiconducting nanoparticles have been the subject of increasing interest since the demonstration in 1975 of the enhancement of their third-order non-linear optical properties [1]. These properties are expected to arise from the confinement of the charge carriers when the particle size becomes of the order of a_B, the Bohr radius of the exciton. A high third-order optical non-linearity of semiconducting nanoparticles should allow a wide range of useful functions, such as high-speed all-optical switching and other signal processing operations. However, such applications require nanoparticles of well-defined dimensions and of sufficiently large concentration. A wide variety of experimental methods has been developed to prepare such confined structures. In particular, technological efforts have been made to improve the epitaxial growth of well-calibrated semiconducting quantum dots [2]. Heteroepitaxial methods are particularly well suited for obtaining many different III-V materials useful for their luminescence properties [3]. Other techniques, such as co-melting [4] or RF co-sputtering [5], are commonly used to produce II-VI semiconductor doped glasses.

More recently, low cost chemical routes have proved to be convenient for generating mono-dispersed nanoparticles in glasses or polymer matrices at low temperatures. In particular, colloidal chemistry and sol-gel techniques can be used to investigate either the intrinsic properties of semiconducting nanoclusters or the influence of a vitreous matrix on these properties. Due to a

difference between the dielectric constant of the particle and that of the surrounding medium, a broadening of the individual exciton features and the appearance of quasi surface states have been predicted theoretically [6], which should be seen in the absorption spectra. Trap surface states, as well as the size dispersion or the electron-phonon interaction are presumed to slow down the resonant non-linearity or to inhibit its oscillator strength. On the other hand, while bulk matrices are useful for studying fundamental effects on the optical properties of the particles, potential technology requires basic spectroscopic research on low-dimensional transparent systems. To obtain a clearer understanding of the relative importance of the matrix on the electronic transitions inside a CdS nanoparticle, we have prepared three types of materials *via* different routes. We have then studied these materials using absorption, emission and Raman spectroscopies.

2. Experimental details

The CdS nanocrystals were generated using three different techniques. The first sample, labelled B_1, consists of a conventional CdS-doped bulk silica xerogel. It was prepared by hydrolysis and polycondensation of trimethoxyorthosilane (TMOS) with H_2O, CH_3OH and dimethylformamide (DMF) in a basic medium [7] (NH_4OH), containing 0.5-at % $Cd(CH_3COO)_2$ as the cadmium precursor. After gelification for about 5 hours, the sample was dried at 35°C and then densified at 600°C using a temperature gradient of 0.1°C/min. A further 2-hour treatment at 200°C under an H_2S gas flow precipitated the CdS in the pores and gave a monolithic yellow transparent glass.

The other two samples were elaborated using a highly concentrated solution of CdS nanoparticles prepared by the inverted micelle method, which has been explained in detail elsewhere [8]. Briefly, the particles were prepared by rapid injection of an excess of H_2S into inverted micelle solutions containing variable amounts of cadmium salt dissolved in the water pools. The inverted micelles were obtained by mixing the appropriate amount of heptane, water, and sodium di-(2-ethylhexyl)sulfoccinate (AOT). After the formation of the CdS nanoparticles, the excess H_2S was removed by bubbling N_2 through the emulsion. Further addition of 4-fluorophenylthiol resulted in the flocculation of the colloid. Finally, centrifugation and drying allowed the recovery of the particles as a powder, which could be dispersed in acetone, leading to a clear yellow solution. The particles size was measured using High Resolution Transmission Electron Microscopy or deduced from the correlation curve between the mean diameter and the exciton peak position in the optical absorption spectrum [9]. CdS colloids with a particle diameter between 1 and 8 nm were thus obtained with a narrow size distribution (less than 10%) and with a concentration up to 15 volume%.

This colloidal solution was used to dope predensified xerogels having a well-calibrated pore size. These porous gel-derived silica monolithic matrices (2.5 mm × 5.6 mm diameter cylinders) were synthesized following a procedure previously reviewed [10]. Careful control of the aging procedure allowed the production of matrices with tailored textural properties. The gels used in this study were 7.8 nm pore-size samples with specific surface areas of 472.7 ± 1.5 m^2/g and pore volumes of $(922 \pm 82) \times 10^{-6}$ m^3/kg as determined by N_2 gas sorption analysis. The pore volume was then used as a host for the active phase. A colloidal solution of CdS nanoparticles was impregnated into the gels by soaking them directly in the solution for one day. We have demonstrated that soaking the gels in acetone does not change their textural properties. After impregnation, the doped gels were dried carefully at 60°C for a few hours. The mean size of the CdS particles contained in this matrix was evaluated at 2 nm from the absorption spectrum of the colloid [8]. The surface of the resulting yellowish gel, labelled B_2, was then carefully cleaned and polished using ethanol and a 1 μm-grain abrasive paper.

The third sample, labeled F consists of a spin coating deposition of the previously mentioned CdS particles on a glass substrate. A sol-gel process for these particles is obtained by oxidation of the thiols under H_2O_2, followed by random aggregation. A polymer (polyvinylpyrrolidone) was added to the initial solution to avoid cracks in the final films. The sol was then spin-coated onto a BK7 glass substrate with a rotation speed of 2500 rpm, which results in an 810 nm-thick layer.

Absorption spectra were recorded at room temperature using a Perkin-Elmer Lambda 19 UV-Vis-IR double-beam spectrophotometer. Considering the high concentration of CdS particles, the bulk samples were polished in order to obtain absorption spectra with a limited saturation effect. For the CdS film, a clean BK7 slide was used as the reference.

Photoluminescence and Raman spectra were carried out at room temperature by exciting the samples resonantly with a number of Ar^+-ion laser lines. The aim of our approach was to excite the nanocrystals resonantly with exciton transition energy close to that of the laser, following the concept of size-selective excitation [11]. In the case of the thin film F in the visible-wavelength domain, the light was focused into a high-refractive index prism pressed onto the film. Under an appropriate angle, a part of the beam energy was then coupled into the waveguide to excite a TE mode. The scattered light emitted at 90° from the sample was then imaged onto the slits of a Jobin-Yvon U1000 monochromator to be analyzed and then detected using a Thorn EMI 9863B photomultiplier.

3. Results and discussion

3.1. Absorption

In Fig. 1 are shown the absorption spectra of the different samples. For all of them, a blue shift of the absorption edge, when compared to the spectrum of bulk CdS, reveals a characteristic confinement effect on the carriers, due to the reduction of the particle size down to nanometric scale. However, it can be noticed that sample B_1 contains larger particles than the other samples. The exciton structure is only visible for film F because of the thickness of the bulk samples, so that the mean size of the nanoparticles in B_1 and B_2 could

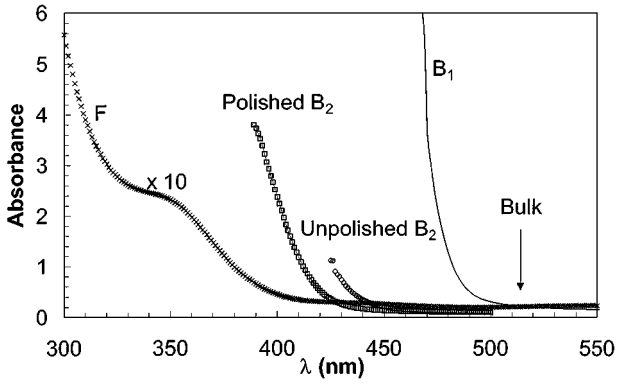

Figure 1 Room temperature optical absorption spectra of samples B_1 (——), B_2 (□), polished B_2 (○) and F (×). Solid arrow indicates the bulk CdS extinction edge.

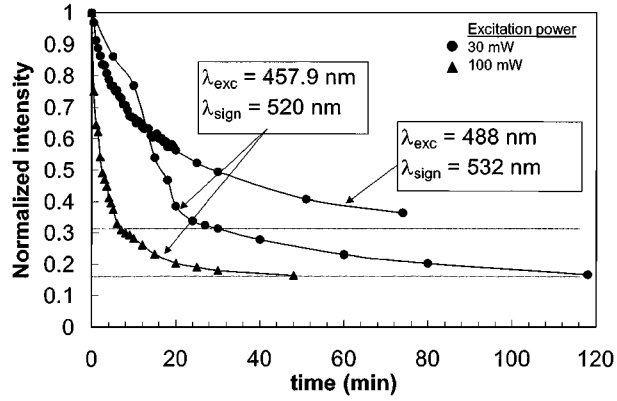

Figure 2 Evolution of the luminescence intensity with the irradiation time for waveguiding configuration in the film F. The symbol shape corresponds to high or low laser power. Both the excitation and detected signal wavelengths are indicated.

not be deduced from these curves. In the spectrum of sample F, the exciton peak around 354 nm leads to the estimation of an average diameter of about 1.8 nm according to the tight-binding model of Lippens and Lannoo [12]. This result is in agreement with the 2 nm size previously measured in the colloidal solution [9]. In the case of sample B_2, even when it was polished down to a thickness of 0.2 mm, the spectrum did not show the exciton, because of the high nanoparticle concentration of 65-vol %. However, the blue shift is more pronounced when the sample is thinned, showing that the smallest particles are found in the core of the host matrix. This fact is easily explained if one considers the impregnation of the colloidal solution as a percolation process in which the diffusion constant differs according to the particle size. It would appear that this matrix plays the role of a sifter for the largest particles, thus narrowing the size distribution.

3.2. Waveguiding in CdS films

To the best of our knowledge, the present work is the first report of waveguiding in an almost pure CdS nanoparticle layer for visible wavelengths. The optical losses have been estimated by numerical analysis of the scattered light from a CdS waveguide and detected by a CCD camera. A considerable attenuation, between 7 and 11 dB/cm, was measured, which depended on the layer thickness. We have determined a refractive index of 1.64 and a mean thickness of 810 nm using the m-line spectroscopic technique, performed at 632.8 nm. The low value of the index compared with the bulk CdS one (≈3) is due mainly to a confinement effect in the semiconductor and to the relative increasing portion of surface ligands when the size is decreased.

However, the waveguiding properties of the CdS layer are sensitive to light. Fig. 2 exhibits the temporal decay of the luminescence signal for several experimental conditions. This decay appears more rapid for the highest laser power (100 mW); while the excitation wavelength influences essentially the asymptote of the signal evolution. For example, the residual intensity remains around 15% for 457.9 nm. Furthermore, it was found that when the laser is shut down during different time delays, the film partly retrieves its waveguiding properties but, after a new irradiation, the signal quickly decreases again to tend towards its initial evolution. This behavior is characteristic of the structural relaxation of the organic molecules but a significant fraction of the signal is permanently photo-degraded by the laser irradiation. Given the optical losses, spectroscopic acquisitions were performed in waveguiding configuration for the highest wavelengths but not in the UV domain. The laser power was kept below 100 mW and a time delay of 30 min was respected between first excitation and measurements, in order to avoid the mentioned photo-degradation.

3.3. Photoluminescence

Photoluminescence (PL) spectra of the different samples and for several laser excitations are shown in Fig. 3. In each case when the laser energy was sufficient for exciting the electron-hole pairs, two emission bands could be distinguished, as already reported in other works [5, 13]. The weak band in the blue region, called band I, corresponds to the direct recombination of the exciton pairs. This band is usually slightly red-shifted when compared to the absorption exciton peak, and the energy shift may reach 0.5 eV, depending on the matrix. Nevertheless, the position of this PL band at 470 nm has led to the evaluation of the particle diameter in sample B_1 as being between 2 and 4.5 nm. This peak seems sharper and more intense in sample F than in the other matrices, showing a more efficient direct recombination in the case of an almost pure form of the CdS particles and making the influence of the host obvious. Clearly, for the nanocrystals prepared by inverted micelle, the interaction between the surface of the pores in the B_2 silica matrix and the complex thiolate particles leads to additional surface depassivation.

The more intense and broader band around 640 nm for sample B_1 and in the green-yellow region for samples B_2 and F, is called band II. It is usually ascribed to the recombination of the excited pairs via trap surface states. In Fig. 3a and b, as the excitation wavelength increases, the largest particles are size-selected and a red shift of the trapped-state band is observed. When the luminescence is not too strong in sample B_1, another band is observable, corresponding to a high-frequency Raman shift of about 4100 cm^{-1}. This band can be assigned to vibrations of organic groups.

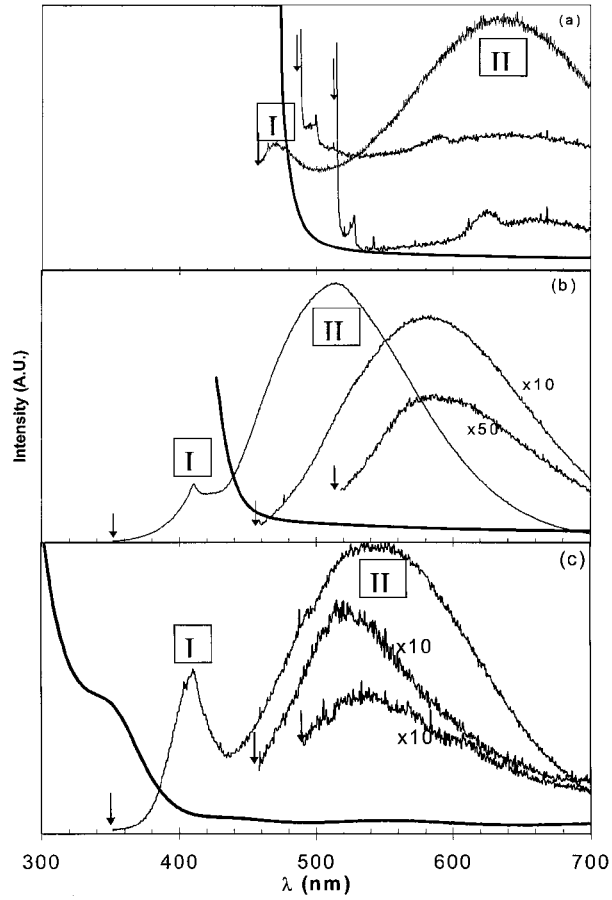

Figure 3 Photoluminescence spectra, taken at excitation wavelengths indicated by the arrows, of samples B_1 (a), B_2 (b) and F (c). Also reported, as thick lines are the corresponding absorption spectra.

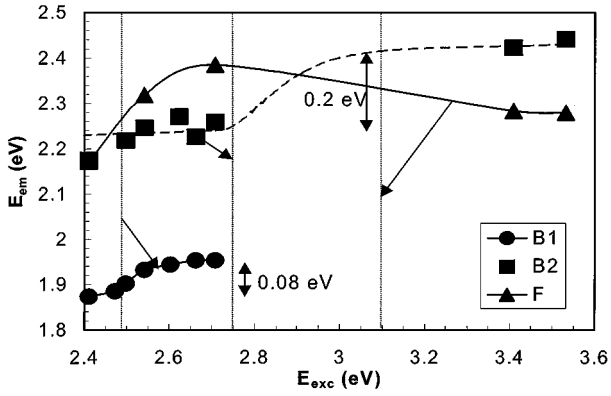

Figure 4 Variation of the energy position of the emission band II as a function of the excitation energy for samples B_1 (●), B_2 (■) and F (▲). The extinction edge is represented for each sample by a vertical dotted line.

In order to clarify the energy levels involved in these transitions, the central position of the band II has been plotted versus the laser excitation energy in Fig. 4. The main tendency is an increase of the emission energy with increasing the excitation one, except for the CdS polymeric film F. However, the shape of the band II in Fig. 3c for UV excitation seems to indicate that it is composed of more than one contribution. As the UV experimental acquisition has not been made in waveguiding configuration, the second contribution probably comes from the substrate. Thus the effective band II for the UV excitations should be located around 2.4 eV.

In the longest wavelength limit, an anomalous decrease of the emission energy, is observed in samples B_2 and F (Fig. 4). This behavior occurs for excitation laser lines strongly out of the absorption domain, so that no particle can be size-selected. Taking into account the weak intensity of this band, we consequently ascribed this luminescence to the surface complexing agent.

The evolution of the energy positions of the emission bands in Fig. 4 can be qualitatively interpreted using a model with two surface trap bands [14]. The corresponding carrier transition mechanisms are shown in the Fig. 5. At the surface of the particle, the donor level situated between the bottom E_C of the conduction band and an energy E_S may be due to an interstitial sulfur [15]. The Acceptor State, more deeply situated inside the band gap, is generally due to an excess of Cd [16]. After absorbing a photon, an electron of the valence band can be excited into the conduction band and then relaxes non-radiatively to the S surface states. When such an electron recombines with a hole of the valence band through a radiative transition, it contributes to the emission band I. If the hole has been activated previously in the Cd trap band, then the recombination electron-hole corresponds to the emission band II. When the laser energy is greater than the gap of the smallest particles, all of the sizes are selected and can be represented by a mean value. In this case, the position of the band II should not depend on

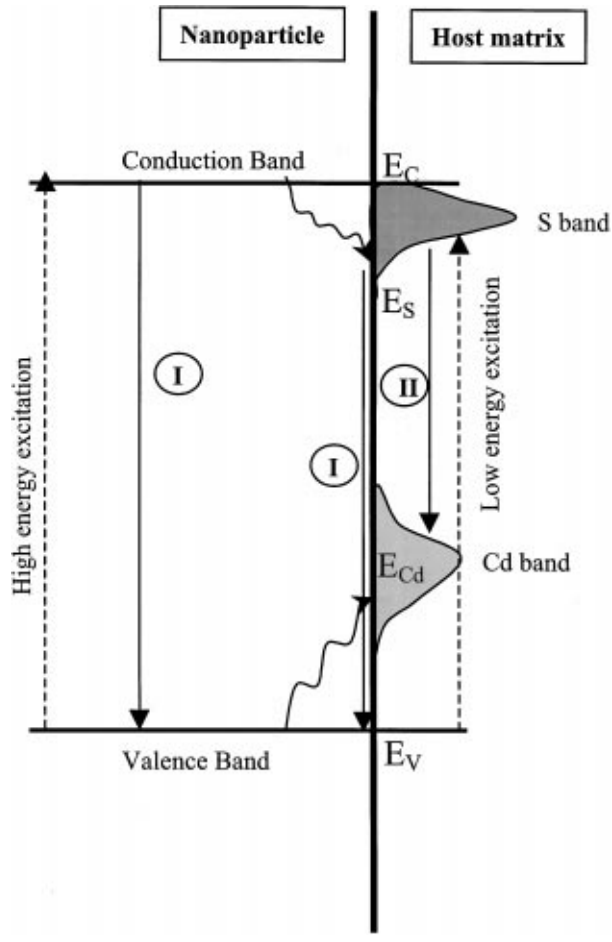

Figure 5 Energy level diagram of the defect states at the nanoparticle surface.

the excitation energy. This fact could be observed in samples B_1 and B_2 in the blue and UV domains, respectively. As the excitation approaches the absorption edge, the particles are size-selected and then the energy of the transition II decreases with decreasing excitation energy, as seen for sample B_1. This result is expected since the shallow S level follows the variation of the conduction edge, which undergoes a larger shift than the valence edge, due to the lower effective mass of the electron ($m_e/m_h = 0.16/5$). Finally, as the excitation energy becomes smaller than the gap of the largest particles, only the S band of these particles is reached by the electrons : the intensity of the type II photoluminescence weakens and its energy position remains almost constant at $E = (E_S - E_{Cd})$. This behavior, observed for sample B_1, can be predicted for sample B_2. Unfortunately, because of a lack of data in the appropriate range, no assumption could be made for the emission band II of the film F. If we assume the mean size of the particles in samples B_1 and B_2 to be equal to 4.5 and 2 nm, respectively, then the energy shift of the emission band II corresponds to a selection between the mean sized nanocrystals and the largest ones. Consequently, we found an estimation of the size dispersion, which is around 3 nm for sample B_1 and only 1 nm for B_2.

3.4. Raman spectroscopy

In semiconducting nanoclusters, the confinement effect is expected to influence the electron-LO phonon interaction also. The exciton-phonon coupling is also assumed to be responsible for the experimentally observed gap between the main lines in absorption and luminescence [17]. Most of the previously reported Raman scattering experiments concerned the phonon confinement or the nature of the electron-phonon coupling [18, 19]. It has been predicted theoretically that the fundamental LO (1LO) frequency should shift to lower energies and that the corresponding band should broaden with decreasing cluster size [20, 21]. However, although the asymmetrical line broadening has been observed systematically in various CdS quantum dots [20, 22], contradictory results have been reported concerning the red-shifted position of this band [19, 20, 23]. In fact, a significant deviation from the bulk 1LO frequency of 305 cm^{-1} has been observed only in CdS_xSe_{1-x} doped glasses [21] and explained as the predominant effect of phonon confinement on the surface strain. As shown in Fig. 6, when the exciting wavelength is far from the excitonic transitions of the sample, no CdS vibrational modes are observed. However, when approaching the resonance conditions, the 1LO mode appears around 302 cm^{-1}. This effect is well observed for the film F (Fig. 6c) where the maximal intensity is obtained for $\lambda_{exc} = 351.1$ nm. The weakness of the observed peak intensities may have two different reasons. In sample B_1 and B_2, the 457.9 nm excitation wavelength is still believed to be too far from resonance to enhance the oscillator strength of the Raman transition. On the other hand, in both the samples B_2 and F, the Raman scattering at 351.1 nm is resonant but the 1LO vibration of CdS is then superimposed on the strong

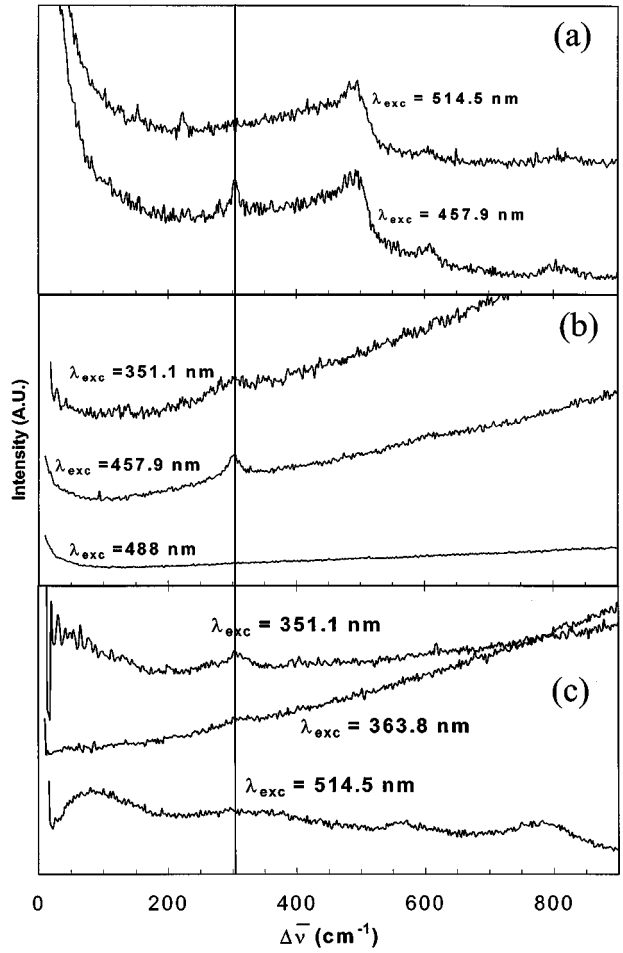

Figure 6 Raman spectra of sample B_1 (a), B_2 (b) and F (c). The excitation wavelength is varied to fulfill resonance conditions.

emission band I. This 1LO Raman cross section enhancement when exciting inside the absorption band has been often reported [20, 24] and theoretically predicted long ago [25]. The resonant transitions of the charge carriers, occurring inside the nanoparticles, allow the normally forbidden LO modes to be active. The experimental frequency of this vibration does not seem to depend on the particle size or the environment of the particles. The theoretically predicted red-shift due to the phonon confinement may be hindered by a blue shift. This second effect would be caused by strain acting on the surface of the nanocrystals, as suggested by Shiang *et al.* [20]. The Raman signal is not strong enough to show the surface phonon mentioned in several works [19, 23, 26].

In non-resonant conditions, the Raman spectra of sample B_1 (Fig. 6a) exhibit the characteristic features of incompletely densified silica xerogels. The amorphous structure of the polymer composing the CdS layer appears in the low energy excitation spectra of sample F (Fig. 6c). Nevertheless, the Raman profile characteristic of the silica matrix could not be seen for sample B_2 (Fig. 6b), probably due to the high porosity of the material.

4. Conclusion

Absorption, photoluminescence and Raman spectroscopies were performed on CdS nanoparticles of

different forms and which had been prepared *via* three different routes. The waveguiding capabilities of almost pure CdS nanocrystalline films were demonstrated, although further progress is still needed in order to stabilize these films and to improve their optical properties. The conventional sol-gel method remains the easiest one for producing semiconducting nanoparticles in silica bulk matrices. However, the particles obtained are rather large and poly-dispersed if the CdS ratio exceeds 1%. Post-doping of porous xerogels seems to provide an interesting method of obtaining well-calibrated and highly concentrated small particles. Yet, interaction between nanocrystals and the SiO_2 matrix, which generates additional trapping energy levels, could be a limiting effect for applications. The two emission bands shown in the luminescence spectra have been interpreted as a direct excitonic recombination and a size-selected transition between the surface trap levels. Quasi-resonant Raman scattering measurements allowed the observation of the 1LO phonon of CdS nanocrystals, even in thin films or at low concentrations. No influence of the matrix or of the particle size on the 1LO vibration has been observed. However, we have shown that clear and intense Raman spectra are difficult to obtain when the exciton recombination occurs because of the emission band I.

Acknowledgements

The Centre d'Etudes et de Recherches Lasers et Applications (CERLA) is supported by the Ministère chargé de la Recherche, the Région Nord-Pas de Calais and the Fonds Européen de Développement Economique des Régions.

References

1. C. FLYTSANIS, in "Quantum Electronics: A Treatise," Vol. 1a (Academic Press, New York, 1975).
2. A. A. GUZELIN, U. BANIN, A. V. KADAVANICH, X. PENG and A. P. ALIVISATOS, *Appl. Phys. Lett.* **69** (1996) 1432.
3. See for example, R. LEON, S. FAFARD, D. LEONARD, J. L. MERZ and P. M. PETROFF, *ibid.* **67** (1995) 521.
4. S. GUHA, V. J. LEPPERT, S. H. RISBUD and I. KANG, *Sol. State Comm.* **105** (1998) 695.
5. A. G. ROLO, O. CONDE and M. J. M. GOMES, *Thin Sol. Films* **318** (1998) 108.
6. E. RABANI, B. HETENYI, B. J. BERNE and L. E. BRUS, *J. Chem. Phys.* **110** (1999) 5355.
7. K. DAHMOUCHE, C. BOVIER and A. BOUKENTER, *J. de Physique iv* **2** (1992) C2.
8. T. GACOIN, L. MALIER and J. P. BOILOT, *Chem. of Mater.* **9** (1997) 1502.
9. T. GACOIN, Thesis (Paris VI, 1994).
10. L. L. HENCH, in "Sol-gel Silica: Processing, Properties and Technology Transfer" (Noyes Publications, New York, 1998).
11. A. EKIMOV, *J. Lumin.* **70** (1996) 1 and references therein.
12. P. E. LIPPENS and M. LANNOO, *Phys. Rev. B* **39** (1989) 10935.
13. S. MOCHIKUZI and K. UMEZAWA, *J. Phys.: Cond. Matter* **8** (1996) 7509.
14. A. HÄSSELBARTH, A. EYCHMÜLLER and H. WELLER, *Chem. Phys. Lett.* **203** (1993) 271.
15. L. S. PEDROTTI and D. C. REYNOLDS, *Phys. Rev. B* **120** (1960) 1664.
16. Y. WANG and N. HERRON, *J. Phys. Chem.* **92** (1988) 4988.
17. P. LAVALLARD, *J. Cryst. Growth* **184/185** (1998) 352.
18. G. SCARMACIO, V. SPAGNOLO, G. VENTRUTI, M. LUGARA and G. C. RIGHINI, *Phys. Rev. B* **53** (1996) R10489.
19. V. PTATSCHEK, B. SCHREDER, K. HERZ, U. HILBERT, W. OSSAU, G. SCHOTTNER, O. RAHAUSER, T. BISCHOF, G. LERMANN, A. MATERNY, W. KIEFER, G. BACHER, A. FORCHEL, D. SU, M. GIERSIG, G. MULLER and L. SPANHEL, *J. Phys. Chem. B* **101** (1997) 898.
20. J. J. SHIANG, S. H. RISBUD and A. P. ALIVISATOS, *J. Chem. Phys.* **98** (1993) 8432.
21. D. BERSANI and P. P. LOTTICI, *Phys. Stat. Sol. (b)* **174** (1992) 575.
22. A. INGALE and K. C. RUSTAGI, *Phys. Rev B* **58** (1998) 7197.
23. K. K. NANDA, S. N. SARANGI, S. N. SAHU, S. K. DEB and S. N. BEHERA, *Physica B* **262** (1999) 31.
24. L. SAVIOT, B. CHAMPAGNON, E. DUVAL and A.I. EKIMOV, *Phys. Rev. B* **57** (1998) 341.
25. M. V. KLEIN and S. P. S. PORTO, *Phys. Rev. Lett.* **22** (1969) 782.
26. K. K. NANDA, S. N. SAHU, R. K. SONI and S. TRIPATHY, *Phys. Rev. B* **58** (1998) 154.

Received 5 August 1999
and accepted 12 October 2000